Materials Transactions, Vol. 59, No. 11 (2018) pp. 1761 to 1766

Growth and Electrical Properties of Epitaxial ZnO Films Prepared by Chemical Bath Deposition Using a Flow Reactor

Masao Miyake*, Ken Yamamoto, Takumi Ikenoue and Tetsuji Hirato

Graduate School of Energy Science, Kyoto University, Kyoto 606-8501, Japan

Deposition methods using aqueous solutions have been developed as cost-effective routes to form transparent ZnO semiconductor films. Chemical bath deposition (CBD) employing a solution of zinc nitrate and hexamethylenetetramine is one of the most popular methods to grow ZnO using aqueous solutions. However, the electrical properties of ZnO films grown by CBD have not been extensively studied. In this study, epitaxial ZnO films were prepared by CBD using a flow reactor under various deposition conditions, and the temperature and reactant concentrations required for the growth of a transparent ZnO film with a smooth surface were determined. The electrical properties of the transparent ZnO films were examined by resistivity and Hall effect measurements. The optimum flow rate of the reaction solution, leading to the fastest growth of ZnO, was also identified. The ZnO film grown at such flow rate exhibited the highest electrical mobility. The carrier concentration and mobility of the ZnO film grown under the optimized conditions were 1.2×10^{18} cm^{-3} and 21 cm^2 V^{-1} s^{-1}, respectively. [doi:10.2320/matertrans.M2018173]

(Received May 25, 2018; Accepted August 2, 2018; Published September 7, 2018)

Keywords: *zinc oxide, chemical bath deposition, epitaxy, carrier concentration, mobility*

1. Introduction

Zinc oxide (ZnO), a semiconductor with a direct bandgap of ~3.4 eV, has many applications, such as transparent conductive contacts, solar cells, photocatalysts, luminescent devices, and ultraviolet detectors.[1–5] In many of these applications, where excellent electrical and optical properties are required, epitaxially grown single-crystal films are preferable to polycrystalline films, due to the electron scattering by grain boundaries in the latter.[6]

Epitaxial ZnO films are generally prepared by vapor-phase processes, including molecular beam epitaxy,[7] pulsed-laser deposition,[8] sputtering,[9] and chemical vapor deposition.[10] However, vapor-phase processes require high temperatures and vacuum conditions, and are therefore expensive. In contrast, deposition processes using aqueous solutions have advantage of being cheaper, as they can be carried out under ambient atmosphere at a relatively low temperature, without expensive equipment.

Among various aqueous solution processes, one of the most popular methods for the deposition of ZnO is low-temperature hydrothermal synthesis, in which ZnO is grown from a ZnO-saturated ammonia aqueous solution by heating, taking advantage of the retrograde solubility of ZnO in the solution.[11–13] The growth of a high-quality single-crystal ZnO film,[14] lateral epitaxial overgrowth,[11] and three-dimensional epitaxy of ZnO[15] have been achieved using this method. Practical applications of these films, such as current-spreading layers[16] and the n-type layer in GaN-based light-emitting diodes,[17] have been studied. Chemical bath deposition (CBD)[1,18] is another popular method for the deposition of ZnO using an aqueous solution. The CBD of ZnO is usually carried out using an aqueous solution containing zinc ion and hexamethylenetetramine (HMT). The hydrolysis of HMT upon heating releases hydroxide ions, which react with zinc ions to form ZnO.[1,19] Although CBD is often used for the preparation of ZnO nanorods or nanowires,[19–23] it can also be applied to grow epitaxial ZnO films.[18] Lateral epitaxial overgrowth was also achieved by CBD.[24,25] As far as morphology and crystalline structure are concerned, both methods seem capable of producing ZnO films of similar quality. However, it is not clear whether the two methods result in ZnO films with similar electrical properties, because only limited results have been reported on the electrical properties of ZnO films prepared by CBD,[18] while a relatively large amount of data is available for films grown by low-temperature hydrothermal synthesis.[11,26–28] In general, electrical properties of a semiconductor strongly depend on the deposition conditions. As the solution environments in which ZnO grows are very different in the two methods, it is possible that they result in ZnO films with different electrical properties.

In this study, we examine the influence of temperature and reactant concentrations on the growth of ZnO epitaxial films by CBD, and identify the deposition conditions under which a transparent epitaxial ZnO film with a smooth surface is formed. Then, we examine the electrical properties of the transparent ZnO film and determine the optimum deposition conditions to obtain a transparent ZnO film with good electrical properties. The CBD process was performed using a flow reactor.[19,28] CBD has been conventionally carried out in batch-type methods, where film growth takes place in a closed system. However, a problem associated with batch-type approaches is that the concentration of reactants in the solution changes as the reaction progresses. A flow reactor resolves this problem by constantly supplying fresh reaction solution to the reaction zone, where the substrate is heated and film growth takes place. Therefore, the flow reactor makes it easier to obtain a film with high uniformity in the growth direction, and to correlate the reaction conditions with the properties of the resulting film. The influences of the flow rate of the reaction solution on the growth and the electrical properties of the ZnO film were also examined.

2. Experimental

An a-plane single crystal sapphire (5 × 7 × 0.43 mm) was used as the substrate for the growth of the ZnO film. Prior to

*Corresponding author, E-mail: miyake.masao.4e@kyoto-u.ac.jp

the ZnO growth by CBD, an epitaxial ZnO seed layer with a thickness of 50 nm was formed on the substrate by magnetron sputtering. The sputtering was performed at a power of 1 kW and a substrate temperature of 500°C under an atmosphere of argon and oxygen at partial pressures of 0.31 Pa and 0.04 Pa, respectively. This seed layer was needed to ensure the adhesion of the ZnO film grown from the aqueous solution onto the substrate.

Aqueous solutions of $Zn(NO_3)_2$ and HMT were used for the CBD of ZnO. The $Zn(NO_3)_2$ solution, with a concentration of 0.02 M–0.12 M, was prepared by dissolving the indicated amount of $Zn(NO_3)_2$ in distilled water, and its pH was adjusted to 2.3 by adding 1 M nitric acid. The HMT solution, with a concentration of 0.05 M–1.2 M, was separately prepared by dissolving HMT in distilled water.

The CBD of ZnO was performed using a custom-built flow reactor with a channel of 20 mm width and 1 mm depth.[28] The details of the flow reactor are reported elsewhere.[28] The substrate was attached to the upper wall of the channel so that it faced downwards, to prevent settling of precipitates on its surface. In order to prevent the formation of bubbles on the substrate surface, a 20-psi inline back-pressure regulator (Upchurch) was installed at the outlet of the reactor.[19] The two reaction solutions described above were loaded separately in two 10-mL syringes and sent into the flow reactor by two syringe pumps (YSP-101, YMC), at the same constant flow rate. The streams of the solutions were merged just before the reactor. The merged solution was flowed through a filter (0.45 μm, 16555 K, Satorius Stedim Biotech), and then introduced into the main channel of the flow reactor. After the reactor was filled with the solution, the temperature of the substrate was increased to the desired deposition temperature at a rate of 1°C min^{-1}. The CBD was performed by holding the flow of the reaction solution and the temperature for 3 h. It should be noted that, as the two solutions were introduced into the reactor at the same flow rate, the concentrations of the reactants were halved after mixing, while the flow rate of the solution was doubled. All concentrations and flow rates reported in this paper denote the values after mixing. The ZnO films grown from the solution were annealed in air at 200°C for 0.5 h using a hotplate (PC-420D, Corning).

X-ray diffraction (XRD) patterns and pole figures of the ZnO films were obtained using an X-ray diffractometer (X'pertPRO-MPD, PANalytical) with Cu Kα radiation. Scanning electron microscopy (SEM; JSM-6510LV, JEOL) was used to inspect the surface morphology and fractured cross-sections of the films. Optical transmittance spectra were measured by an ultraviolet-visible spectrometer (UV-2450, Shimadzu). Electrical properties were measured with a resistivity/Hall measurement system (ResiTest 8300, Toyo Corporation) using the van der Pauw method.

3. Results and Discussion

3.1 Appearance and morphology of ZnO films

3.1.1 Growth temperature

ZnO formation by CBD using a solution of $Zn(NO_3)_2$ and HMT ($C_6H_{12}H_4$) has been reported to proceed according to the following reactions:[1,19]

$$C_6H_{12}H_4 + 6H_2O \rightarrow 6HCHO + 4NH_3 \quad (1)$$

$$NH_3 + H_2O \rightarrow NH_4^+ + OH^- \quad (2)$$

$$2OH^- + Zn^{2+} \rightarrow ZnO(s) + H_2O \quad (3)$$

The reactions are triggered by the hydrolysis of HMT upon heating to release ammonia (eq. (1)), which produces OH^- (eq. (2)) and drives the growth of ZnO (eq. (3)). The growth rate, morphology, and properties of the resulting ZnO are expected to be affected by various deposition conditions, such as the temperature and the concentrations of $Zn(NO_3)_2$ and HMT.

The effect of the temperature on the growth of the ZnO films was examined by varying the growth temperature in the range from 25°C to 90°C. The reaction solution containing 0.04 M $Zn(NO_3)_2$ and 0.4 M HMT was employed in these experiments. The reactions carried out at temperatures higher than 70°C resulted in hazy white films, while transparent films were formed or no deposition occurred at temperatures of 60°C or lower. The cross-sectional SEM image of the sample after the reaction at 30°C (Fig. 1(a), inset) confirms that ZnO did not grow at this temperature, as the thin layer observed on the substrate had a thickness of 50 nm, which is the same as that of the ZnO seed layer prepared by sputtering prior to the CBD. At temperatures higher than 40°C, the thickness of the ZnO film increased with increasing temperature (Figs. 1(b)–1(f), inset). In other words, the growth rate increased with increasing temperature. At 60°C, the thickness of the ZnO film increased up to ~1 μm during a reaction time of 3 h. The SEM images show that ZnO films with a relatively smooth surface were formed in the temperature range of 40–60°C, although some particles, which seemed to have been generated in the bulk solution before settling down on the surface of the growing ZnO film,

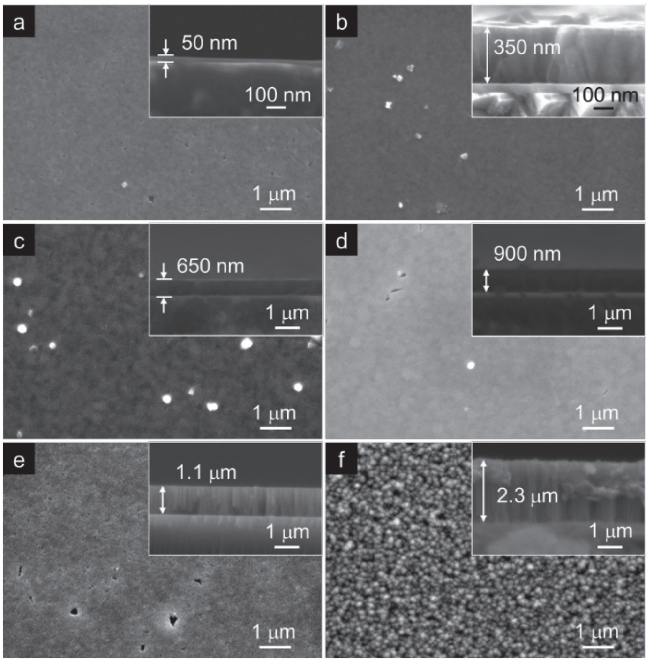

Fig. 1 SEM images of ZnO films grown at various temperatures: (a) 30°C, (b) 40°C, (c) 50°C, (d) 60°C, (e) 70°C, and (f) 90°C. The insets show fractured cross-sections of the ZnO films. The ZnO films were grown from a solution containing 0.08 M $Zn(NO_3)_2$ and 0.8 M HMT. The flow rate of the solution was 10 μL min^{-1}.

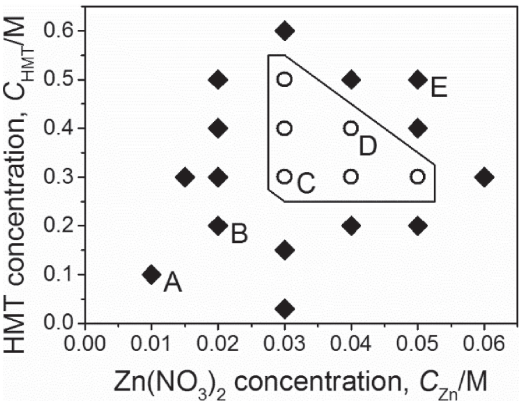

Fig. 2 Diagram showing the appearances of ZnO films grown from solutions with different concentrations of $Zn(NO_3)_2$ and HMT. The ZnO films were grown at a temperature of 60°C and a flow rate of 10 μL min^{-1}. The ○ and ◆ symbols denote concentrations that yielded transparent and hazy films, respectively.

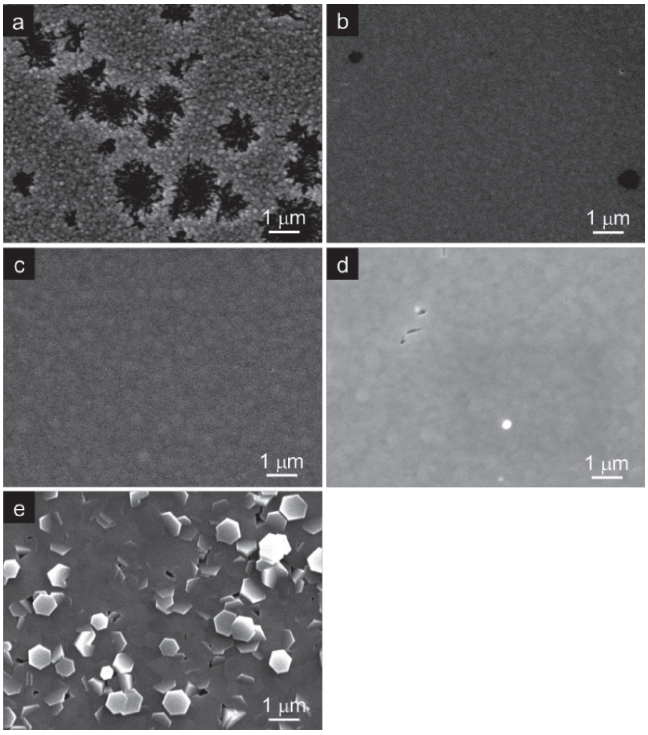

Fig. 3 Surface SEM images of ZnO films grown from solutions with different concentrations of $Zn(NO_3)_2$ and HMT. The HMT/$Zn(NO_3)_2$ concentration ratio was fixed to 10 and the concentration of $Zn(NO_3)_2$ was (a) 0.01 M, (b) 0.02 M, (c) 0.03 M, (d) 0.04 M, and (e) 0.05 M. The growth temperature and flow rate were 60°C and 10 μL min^{-1}, respectively.

were also observed (Figs. 1(b)–1(d)). Rougher surfaces were observed at 70°C, as voids of several hundred nanometers in size were observed on the surface of the film (Fig. 1(e)). The roughest surface, composed of crystal grains with diameter of 200 nm, was formed at 90°C (Fig. 1(f)). A transparent film with a smooth surface was obtained at 60°C, and the films became hazy at higher temperatures. The growth temperature of 60°C was thus employed in the subsequent experiments.

3.1.2 Concentrations of reactants

A wide range of combinations of $Zn(NO_3)_2$ and HMT concentrations was tested at 60°C, to identify those that lead to the formation of transparent ZnO films. Figure 2 identifies the appearance (transparent or hazy) of the ZnO films grown from solutions with different HMT and $Zn(NO_3)_2$ concentrations (reported in the vertical and horizontal axes of the figure, respectively). The diagram identifies a range of combinations of $Zn(NO_3)_2$ and HMT concentrations that yielded transparent ZnO films; hazy films were formed outside this range.

In order to clarify the influence of the concentrations of the reactants on the morphology of the film, we focus on the films from the solutions indicated by A–E in Fig. 2, as representative examples. In these solutions, the concentrations of $Zn(NO_3)_2$ and HMT varied from 0.01 to 0.05 M and 0.1 to 0.5 M, respectively, while the $Zn(NO_3)_2$/HMT concentration ratio was kept at 1:10. As shown in Fig. 2, transparent ZnO films were obtained from the solutions with 0.03 and 0.04 M $Zn(NO_3)_2$ (labeled C and D, respectively), whereas hazy films were formed from solutions with lower or higher concentrations (A, B, and E). The surface SEM images of these films (Fig. 3) show that, at low concentrations, large voids with diameters larger than 500 nm were formed in the deposited ZnO films (Figs. 3(a) and 3(b)). At $Zn(NO_3)_2$ and HMT concentrations of 0.03 M 0.3 M, respectively, a flat and smooth ZnO film without voids and precipitates settling on the surface was obtained (Fig. 3(c)). A further increase in the concentration resulted again in the formation of small voids in the film (Fig. 3(d)). Finally, at the highest concentrations, a rough surface composed of randomly oriented, well-faceted hexagonal crystal grains of ZnO was formed (Fig. 3(e)). The transparent appearance of the films corresponds to a flat surface with fewer voids, whereas scattering of light by a rough surface and voids is responsible for the hazy appearance of the corresponding films.

The formation of voids in the films grown from solutions A and B indicates that the concentrations of the reactants in these solutions were too low. The small voids formed at high concentrations (solution D) are ascribed to the preferential growth of the ZnO crystal in the c-axis direction, i.e., to a relatively weak growth of the ZnO crystal in the lateral direction. As shown by the XRD analysis below, the grown ZnO crystal is c-axis oriented, and has a general tendency to grow preferentially in the c-axis direction.[29] When the concentration of the reactants is further increased (solution E), the driving force for the ZnO deposition becomes too high, and new nuclei with crystal orientations unrelated to the seed layer can thus be generated. As a result, a randomly oriented polycrystalline ZnO film is formed. A smooth ZnO film without voids can be obtained for appropriate reactant concentrations (solution C).

The transparency of the films can be confirmed by examining the optical transmittance spectra in Fig. 4. The spectra show that all films have an optical absorption edge at 360–380 nm, corresponding to a bandgap of 3.3–3.4 eV. The transparent or hazy appearance of the films depends on the transmittance in the wavelength range of 400–800 nm. In this wavelength range, the transparent films exhibit a transmittance as high as 70–80%, whereas that of the hazy films is lower than 70%. Fabry–Perot fringes are clearly observed in the spectra of the films obtained from high-concentration solutions (solutions C, D, and E), indicating

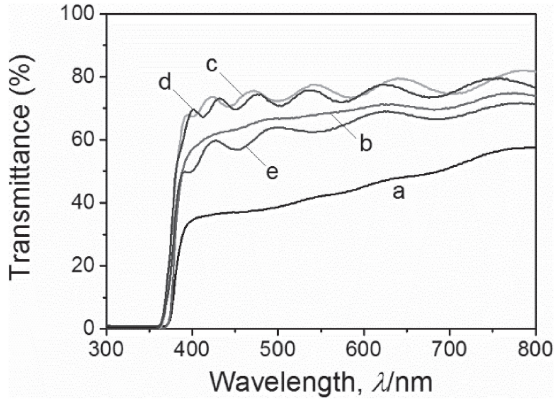

Fig. 4 Optical transmittance spectra of ZnO films grown from solutions containing (a) 0.01 M, (b) 0.02 M, (c) 0.03 M, (d) 0.04 M, and (e) 0.05 M $Zn(NO_3)_2$, together with HMT at concentrations 10 times higher than $Zn(NO_3)_2$. The deposition temperature and the flow rate were 60°C and 10 μL min^{-1}, respectively.

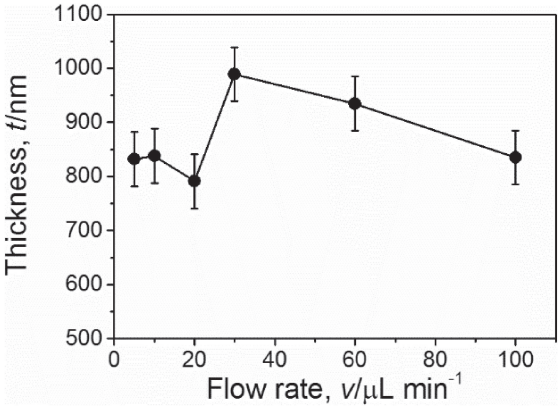

Fig. 5 Thickness of ZnO film grown after 3 h of reaction at various flow rates. The ZnO films were grown at 60°C using a solution containing 0.03 M $Zn(NO_3)_2$ and 0.3 M HMT. The thickness of the film was estimated from the optical transmittance spectrum.

that the films have a relatively small surface roughness and a uniform thickness over the measurement area. The thickness of the ZnO film was estimated from the fringe spacing, based on the assumption that the refractive index of the film matched that determined by Bond.[30] The thicknesses of the films grown from solutions C, D, and E were calculated to be 840, 920, and 770 nm, respectively, in good agreement with the values obtained from the cross-sectional SEM images (see Fig. 1(d) for the film grown from solution C).

3.1.3 Flow rate of reaction solution

The growth rate and morphology of ZnO can also be affected by the flow rate of the reaction solutions. The influence of the flow rate was examined using solution C. At every flow rate examined in this study (5–100 μL min^{-1}), a transparent ZnO film was obtained from the solution. No significant differences in the morphologies of the films obtained at different flow rates were highlighted by SEM images. However, the thickness of the film varied with the flow rate (Fig. 5). As the reaction time was kept constant, the thickness of the film is representative of the growth rate. The highest growth rate was obtained at the flow rate of 30 μL min^{-1}. In the low flow rate range, a faster growth was observed with increasing flow rate; this indicates that the growth rate is controlled by feeding rate of the reactants to the surface of the growing ZnO crystal. However, when the flow rate was too high, the growth rate decreased. This decrease in growth rate is probably due to the reactant ions being swept downstream before completing the ZnO formation reaction.

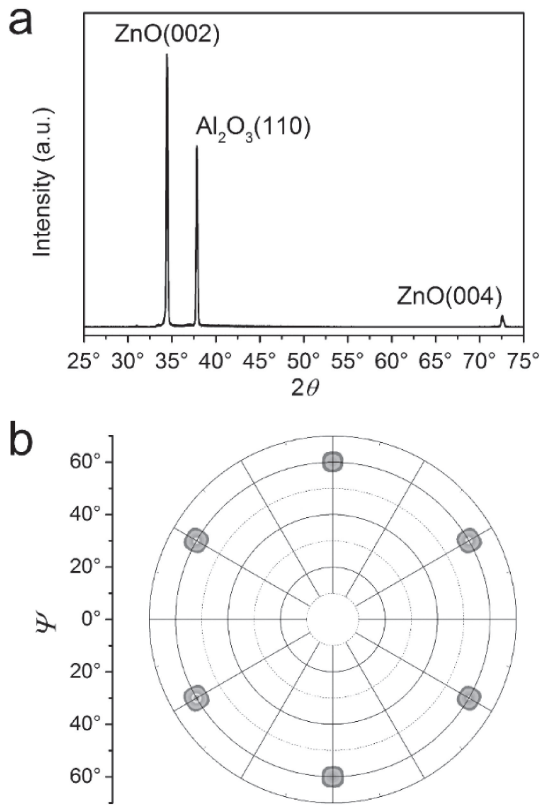

Fig. 6 Typical (a) XRD θ–2θ scan and (b) ZnO (101) pole figure of a ZnO film prepared in this study.

3.2 Epitaxy

Figure 6 shows the typical XRD pattern of a transparent film obtained by CBD. The XRD pattern recorded in θ–2θ scan mode shows only the ZnO (002) and ZnO (004) diffraction peaks, besides the sapphire substrate peak. The ZnO (101) pole figure reveals a clear six-fold symmetric pattern of the diffraction peaks at a tilt angle (Ψ) of ~60°, confirming that the transparent film was composed of single-phase, epitaxially grown ZnO.

3.3 Electrical properties

The electrical properties of the transparent ZnO films grown from the solutions indicated by open circles in Fig. 2 are listed in Table 1. These properties were obtained for films after annealed at 200°C for 30 min. The electrical resistivities of the as-grown ZnO films were over 10^6 Ω cm and the Hall voltage of these films could not be obtained. After annealing, the resistivity drastically decreased by the order of magnitude of over 10^4. The lowest resistivity was obtained for the film grown from solution C, containing 0.03 M $Zn(NO_3)_2$ and 0.3 M HMT. This ZnO film also exhibited the highest carrier concentration and mobility. Both carrier concentration and mobility showed a decreasing trend with increasing $Zn(NO_3)_2$ and HMT concentrations. The Hall voltage for the

Table 1 Electrical properties of ZnO films grown from reaction solutions with different concentrations of $Zn(NO_3)_2$ and HMT.

Concentrations of reactants, *C*/M		Resistivity,	Carrier	Mobility,
$Zn(NO_3)_2$	HMT	ρ/Ω cm	concentration, n/cm^{-3}	$\mu/cm^2\,V^{-1}\,s^{-1}$
0.03	0.3	0.56	7.2×10^{17}	16
0.04	0.3	26	5.6×10^{16}	4.4
0.05	0.3	190	—*	—*
0.03	0.4	14	1.3×10^{17}	3.3
0.04	0.4	36	—*	—*
0.03	0.5	25	7.0×10^{16}	3.6

* Data could not be measured.
All films were grown at 60 °C and the flow rate of the reaction solution was 10 μL min^{-1}. The electrical properties were measured after annealing at 200 °C.

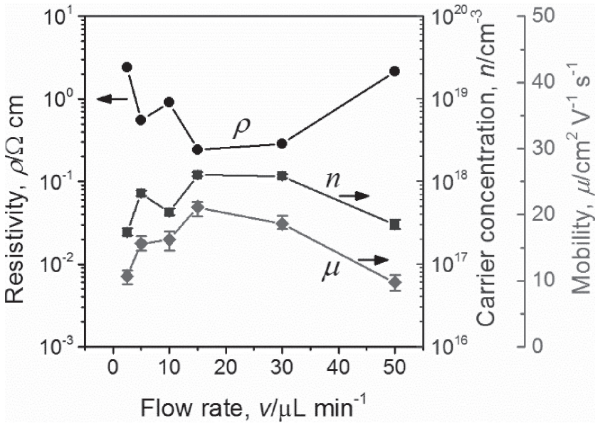

Fig. 7 Resistivity, carrier density, and mobility of ZnO films grown at various flow rates. The ZnO films were grown at 60°C using a solution containing 0.03 M $Zn(NO_3)_2$ and 0.3 M HMT.

films grown from solutions with higher concentrations of $Zn(NO_3)_2$ and HMT was too small to be measured, indicating that the mobility of these films was too low. The decrease in both carrier concentration and mobility suggests that a larger number of defects that trap electrons were formed in the ZnO film. The optimum concentrations, leading to the formation of the ZnO film with the best electrical properties, were 0.03 M $Zn(NO_3)_2$ and 0.3 M HMT (solution C).

Figure 7 shows the electrical properties of the ZnO films obtained from solution C at various flow rates. The figure shows that the highest carrier concentration, mobility, and thus lowest resistivity values ($1.2\times10^{18}\,cm^{-3}$, $21\,cm^2\,V^{-1}\,s^{-1}$, and $0.2\,\Omega$ cm, respectively) were obtained at the flow rate of 30 μL min^{-1}. The trend of carrier concentration and mobility with respect to the flow rate was similar to that of the growth rate of the film. This indicates that the ZnO crystal grows efficiently at the optimum flow rate, and a crystal with fewer structural defects and thus good electrical properties is grown under such conditions.

The highest electrical mobility obtained in this study ($21\,cm^2\,V^{-1}\,s^{-1}$) is almost the same as that reported by Hamada *et al.* for a ZnO film epitaxially grown on a sapphire substrate by CBD ($22.6\,cm^2\,V^{-1}\,s^{-1}$). However, higher mobilities ($58–71\,cm^2\,V^{-1}\,s^{-1}$) have been achieved in ZnO films grown by low-temperature hydrothermal synthesis.[15,16,28] This difference in electrical properties may originate from the different pH of the reaction solutions employed in the two methods: the pH is higher for the solution used in the low-temperature hydrothermal synthesis. It has been reported that ZnO crystals grown from aqueous solutions contain a small amount of hydroxide ions as impurities, which can reduce the mobility of electrons in the crystal.[26,31] The amount of hydroxide ions incorporated in ZnO during the crystal growth is expected to depend on the pH of the reaction solution.

4. Conclusions

In summary, ZnO films were grown by CBD using HMT and $Zn(NO_3)_2$ solutions with a flow reactor. ZnO grew at temperatures higher than 40°C, and transparent ZnO films were obtained at temperatures of 60°C or lower. The films obtained from the solution with 0.04 M $Zn(NO_3)_2$ and 0.4 M HMT at temperatures higher than 60°C had a hazy appearance. We determined the range of HMT and $Zn(NO_3)_2$ concentrations in which transparent epitaxial ZnO films can be obtained at 60°C. The flow rate of the reaction solution resulting in the highest ZnO growth rate was also determined. The ZnO film with the best electrical properties (resistivity of $0.2\,\Omega$ cm, carrier concentration of $1.2\times10^{18}\,cm^{-3}$, and mobility of $21\,cm^2\,V^{-1}\,s^{-1}$) observed in this study was obtained from the solution with 0.03 M $Zn(NO_3)_2$ and 0.3 M HMT, at the flow rate of 30 μL min^{-1}.

Acknowledgement

This work was supported by JSPS KAKENHI Grant Number 17K18988.

REFERENCES

1) L. Schmidt-Mende and J.L. MacManus-Driscoll: Mater. Today **10** (2007) 40–48.
2) S.G. Kumar and K.S.R.K. Rao: RSC Advances **5** (2015) 3306–3351.
3) A.B. Djurišić, X. Liu and Y.H. Leung: Phys. Status Solidi Rapid Res. Lett. **8** (2014) 123–132.
4) K.M. Lee, C.W. Lai, K.S. Ngai and J.C. Juan: Water Res. **88** (2016) 428–448.
5) J.H. Choy, E.S. Jang, J.H. Won, J.H. Chung, D.J. Jang and Y.W. Kim: Adv. Mater. **15** (2003) 1911–1914.
6) A. Janotti and C.G. Van de Walle: Rep. Prog. Phys. **72** (2009) 126501.
7) X.H. Wei, Y.R. Li, J. Zhu, W. Huang, Y. Zhang, W.B. Luo and H. Ji: Appl. Phys. Lett. **90** (2007) 151918.
8) E.M. Kaidashev, M. Lorenz, H. Von Wenckstern, A. Rahm, H.C. Semmelhack, K.H. Han, G. Benndorf, C. Bundesmann, H. Hochmuth and M. Grundmann: Appl. Phys. Lett. **82** (2003) 3901–3903.
9) Y.J. Kim, Y.T. Kim, H.K. Yang, J.C. Park, J.I. Han, Y.E. Lee and H.J. Kim: J. Vac. Sci. Technol. A **15** (1997) 1103–1107.
10) M.M.C. Chou, L.W. Chang, H.Y. Chung, T.H. Huang, J.J. Wu and C.W. Chen: J. Cryst. Growth **308** (2007) 412–416.
11) D. Andeen, J.H. Kim, F.F. Lange, G.K.L. Goh and S. Tripathy: Adv. Funct. Mater. **16** (2006) 799–804.
12) J.J. Richardson and F.F. Lange: Cryst. Growth Des. **9** (2009) 2570–2575.
13) J.J. Richardson and F.F. Lange: Cryst. Growth Des. **9** (2009) 2576–2581.
14) D. Andeen, L. Loeffler, N. Padture and F.F. Lange: J. Cryst. Growth **259** (2003) 103–109.

15) M. Miyake, M. Suginohara, N. Narahara, T. Hirato and P.V. Braun: Chem. Mater. **29** (2017) 9734–9741.
16) A.H. Reading, J.J. Richardson, C.-C. Pan, S. Nakamura and S.P. DenBaars: Opt. Express **20** (2012) A13–A19.
17) H.Q. Le, S.K. Lim, G.K.L. Goh, S.J. Chua, N.S.S. Ang and W. Liu: Appl. Phys. B **100** (2010) 705–710.
18) T. Hamada, A. Ito, E. Fujii, D. Chu, K. Kato and Y. Masuda: J. Cryst. Growth **311** (2009) 3687–3691.
19) K.M. McPeak and J.B. Baxter: Ind. Eng. Chem. Res. **48** (2009) 5954–5961.
20) V. Consonni, E. Sarigiannidou, E. Appert, A. Bocheux, S. Guillemin, F. Donatini, I.C. Robin, J. Kioseoglou and F. Robaut: ACS Nano **8** (2014) 4761–4770.
21) T. Cossuet, E. Appert, J.-L. Thomassin and V. Consonni: Langmuir **33** (2017) 6269–6279.
22) R. Nandi, R.S. Srinivasa and S.S. Major: Mater. Chem. Phys. **182** (2016) 155–166.
23) J.J. Hassan, M.A. Mahdi, A. Ramizy, H. Abu Hassan and Z. Hassan: Superlattices Microstruct. **53** (2013) 31–38.
24) H. Chen, H. Wang and X. Lin: J. Alloys Compd. **707** (2017) 341–346.
25) R.M. Ko, Y.R. Lin, C.Y. Chen, P.F. Tseng and S.J. Wang: Curr. Appl. Phys. **18** (2018) 1–11.
26) J.J. Richardson, G.K.L. Goh, H.Q. Le, L.-L. Liew, F.F. Lange and S.P. DenBaars: Cryst. Growth Des. **11** (2011) 3558–3563.
27) H.Q. Le, S.K. Lim, G.K.L. Goh, S.J. Chua, N.S.S. Ang and W. Liu: Appl. Phys. B **100** (2010) 705–710.
28) M. Miyake, H. Fukui, T. Doi and T. Hirato: J. Electrochem. Soc. **161** (2014) D725–D729.
29) K.M. McPeak and J.B. Baxter: Cryst. Growth Des. **9** (2009) 4538–4545.
30) W.L. Bond: J. Appl. Phys. **36** (1965) 1674–1677.
31) M. Miyake, S. Inudo, T. Doi and T. Hirato: Mater. Chem. Phys. **190** (2017) 146–152.